Final Draft
of the original manuscript:

Zou, A.; Li, Y.; Chen, Y.; Angelova, A.; Haramus, V.M.; Li, N.; Drechsler, M.; Angelov, B.; Gong, Y.:

Self-assembled stable sponge-type nanocarries for Brucea javanica oil delivery

In: Colloids and Surfaces B (2017) Elsevier

DOI: 10.1016/j.colsurfb.2017.02.031

Self-assembled stable sponge-type nanocarries for *Brucea javanica* oil delivery

Aihua Zou [a#*] Yawen Li[a#], Yiyin Chen[a], Angelina Angelova[b], Vasil M. Garamus[c], Na Li[d], Markus Drechsler [e], Borislav Angelov [f], Yabin Gong[g]

[a] *Shanghai Key Laboratory of Functional Materials Chemistry, State Key Laboratory of Bioreactor Engineering and Institute of Applied Chemistry, School of Chemistry and Molecular Engineering, East China University of Science and Technology, Shanghai 200237, P. R. China*

[b]*Institut Galien Paris-Sud, CNRS UMR 8612, Univ. Paris-Sud, Université Paris-Saclay, LabEx LERMIT, F-92296 Châtenay-Malabry cedex, France,*

[c]*Helmholtz-Zentrum Geesthacht, Centre for Materials and Coastal Research, D-21502 Geesthacht, Germany*

[d] *National Center for Protein Science Shanghai and Shanghai Institute of Biochemistry and Cell Biology, Shanghai 200237, P. R. China*

[e]*Laboratory for Soft Matter Electron Microscopy, Bayreuth Institute of Macromolecular Research (BIMF), University of Bayreuth, D-95440 Bayreuth, Germany*

[f]*Institute of Physics, ELI Beamlines, Academy of Sciences of the Czech Republic, Na Slovance 1999/2, CZ-18221 Prague, Czech Republic,*

[g]*Yueyang Hospital of Integrated Traditional Chinese and Western Medicine, Shanghai University of Traditional Chinese Medicine, Shanghai 200437, P.R. China*

[*]To whom correspondence should be addressed.
Tel/Fax: +86-21-64252231
E-mail: aihuazou@ecust.edu.cn.
[†]East China University of Science and Technology.
[#]These authors contributed equally to this work

Abstract

Sponge-type nanocarriers (spongosomes) are produced upon dispersion of a liquid crystalline sponge phase formed by self-assembly of an amphiphilic lipid in excess aqueous phase. The inner organization of the spongosomes is built-up by randomly ordered bicontinuous lipid membranes and their surfaces are stabilized by alginate chains providing stealth properties and colloidal stability. The present study elaborates spongosomes for improved encapsulation of *Brucea javanica* oil (BJO), a traditional Chinese medicine that may strongly inhibit proliferation and metastasis of various cancers. The inner structural organization and the morphology characteristics of BJO-loaded nanocarriers at varying quantities of BJO were determined by cryogenic transmission electron microscopy (Cryo-TEM) ,small angle X-ray scattering (SAXS) and dynamic light scattering (DLS). Additionally, the drug loading and drug release profiles for BJO-loaded spongosome systems also were determined. We found that the sponge-type liquid crystalline lipid membrane organization provides encapsulation efficiency rate of BJO as high as 90%. *In vitro* cytotoxicity and apoptosis study of BJO spongosome nanoparticles with A549 cells demonstrated enhanced anti-tumor efficiency. These results suggest potential clinical applications of the obtained safe spongosome formulations.

Keywords: nanosponges, liquid crystalline nanocarriers, self-assembly, phytochemical anticancer nanomedicines

Introduction

Development of nanosized drug delivery systems for Chinese herbal medicines has received considerable attention over the past years [1-10]. Nanoformulations such as nanoemulsions, liposomes, polymeric nanoparticles, and lyotropic liquid crystalline nanoparticles have been used for encapsulation of Chinese herbal medicines and have demonstrated remarkable advantages over conventional formulations [1-11].

Brucea javanica seed oil (BJO) is a traditional herbal medicine with antitumor activity resulting from synergistic effects of its oleic and linoleic acid constituents, anthraquinone, and tetracyclic triterpene quassinoids [2,3] (see ESI, Fig. S1). BJO is extracted from the seeds of *Brucea javanica* (L.) through a circulation extraction method in petroleum ether [2]. Oleic and linoleic acids are the main bioactive components of BJO [3]. Previous studies have reported that BJO may induce apoptosis at low concentrations, while it induces necrosis at elevated concentrations [4]. At the subcellular level, BJO provokes apoptosis through both mitochondrial and death receptor pathways [5]. Moreover, BJO can arrest the cell cycle in the G0/G1 phase [6,7] and thus it enables the inhibition of the cancer cell growth.

BJO is practically insoluble in water. Different delivery systems have been proposed for improvement of its absorption and bioavailability towards tumor treatment. *Brucea javanica* oil emulsion (BJOE) has been clinically used to treat carcinomas since many years in China [8]. Its clinical applications have included lung, prostate, and gastrointestinal cancers [8-10]. BJOE has found limited applications as an oral formulation because of its unpleasant smell causing patients discomfort. BJO-loaded liposomes have been prepared as a potential BJO delivery system of nanosized dimensions in antitumor therapy, but the achieved drug loading of 3.6% has been found insufficient [12]. Nanostructured lipid carriers have permitted to increase BJO loading to a value of 10.4% [13]. Ongoing research on BJO nanoencapsulation and carrier systems should still resolve the shortcomings of low drug loading and poor aqueous solubility.

Recently, liquid crystalline lipid nanocarriers have been utilized in the nanomedicine field for different applications including the development of

theranostics [14-35]. They are also attractive nanocarriers for solubilizing nutraceuticals and functional foods [17-37]. Moreover, they have received increased attention for drug delivery purposes due to their high capacity for encapsulation of active molecules, potential to protect the therapeutic compounds from degradation, and sustained release properties [36-75]. Biomolecular self-assembly has been used in the design of different innovative drug delivery systems [15-18,49,60-75]. Drug-loaded nanoparticles have been obtained from self-assembled liquid crystalline phases upon surfactant-assisted dispersion under physical agitation [15-18,36-56,67]. The agitation methods for generation of fine and uniform dispersions of liquid crystalline nanoparticles usually include high energy input devices, *e.g.* combinations of magnetic stirring, vortexing, sonication bath, pulsed sonication, high pressure/high shear microfluidic homogenization, and heating in autoclave [14-24,65-69,74,75]. Guest molecules have been embedded in either ordered or random channel network architectures constituting the biocompatible liquid crystalline nanocarriers [19,29,50,55-65]. The small angle X-ray and neutron scattering methods have been broadly employed towards controlled fabrication of drug delivery systems [14-22,27-39,49-51,54-58,66,67,76-80]. The obtained structural knowledge has been valuable for optimization of the nanocarriers stability and loading capacity (aqueous hydrophilic channel compartments and lipid hydrophobic compartments).

The aim of the present study is to design and prepare stable sponge-type liquid crystalline nanodelivery systems of BJO [BJO-spongosomes] with nanodimensional sizes, high drug upload, and optimized cytotoxicity. Self-assembled liquid crystalline mixtures of the amphiphilic lipid glycerol monooleate (GMO) were dispersed *via* the surfactant polysorbate 80 (P80). It was taken into account that P80 is not very efficient solubilizer of the bicontinuous membranes of GMO in the absence of oil additives and that stable colloidal dispersions can be obtained upon incorporation of amphiphilic substances [33,65-67,73]. We determined the encapsulation efficiency of various amounts of BJO in spongosome nanocarriers. Morphologies and high-resolution structural characteristics of the BJO-loaded nanoparticles were determined by cryogenic transmission electron microscopy and SAXS. The sustained

drug release properties of the nanocarriers were evaluated in connection with the investigated biological effects. The A549 cells were investigated as a model of cancer cells pathology.

Materials and methods

1. Materials

Brucea javanica seed oil (BJO) was received as a generous gift from Yan'an Changtai Pharmaceutical Co., Ltd. (China) and was used as received. Information obtained from the supplier indicated that BJO comprises 63.3% oleic acid and 21.2% linoleic acid. Glycerol monooleate (GMO) was obtained from General-Reagent Co. Ltd. (China). Alginic acid sodium salt, polysorbate 80 (P80) and 3-(4,5-dimethylthiazol-2-yl)-2,5-diphenyltetrazolium bromide (MTT) were purchased from Sigma Aldrich (USA). Hoechst 33342 was provided by Beyotime Biotechnology Company (China). All experiments were performed in phosphate buffered saline (PBS) with a concentration of 0.01M at pH 7.4. The water used in the experiment was double distilled.

2. Sample preparation

Table 1 presents the compositions studied for spongosome nanoparticle fabrication. Samples were prepared using a modification of a previously reported protocol [11]. Briefly, GMO was melted and mixed with the fluid-phase P80 to prepare a homogeneous GMO/P80 blend. The weight ratio for the GMO/P80 mixture was 22/33. Vortex and sonication steps we employed followed by high-pressure homogenization for the sake of fragmentation of the lipid mixtures and low polydispersity of the obtained dispersions. Practically, the GMO/P80 blend was hydrated, after cooling to room temperature, with appropriate volumes of buffer solution (PBS pH 7.4, 0.5 wt% sodium alginate) by applying vortex shaking every 10 minutes during 1 hour. The dispersions were further stirred intensely at 10 000 rpm

for 1 min and sonicated in ice bath for 15 min. Then, the dispersions were processed through a high-pressure homogenizer apparatus (HPH ATS Engineering, Canada) for five homogenization cycles performed at 850 bars. Samples loaded with BJO were prepared using the same procedure for different amounts of BJO in the lipid mixtures (Table 1).

Table 1. Compositions of liquid crystalline systems used for preparation of drug-loaded spongosome dispersions.

Sample	GMO (mg)	P80 (mg)	BJO (mg)
BJO-2[#]	500	66.7	100
BJO-5	500	66.7	250
BJO-10	500	66.7	500
Blank	500	66.7	-

[#]The sample codes BJO-2, BJO-5, BJO-10 correspond to total BJO concentrations in the samples of 2 mg/ml, 5 mg/ml, and 10 mg/ml, respectively. The aqueous phase volume was 50 mL.

3. Nanoparticle size and zeta potential

The mean hydrodynamic nanoparticle diameters, nanoparticle size distributions, and zeta potentials of the samples were determined by dynamic light scattering (DLS) and zeta potential measurements using a Delsat Nano C Particle Analyzer (Beckman Coulter, USA). Prior to analysis, samples were diluted with PBS (1:10) to avoid additional scattering effects caused by high turbidity of the dispersions. Measurements were performed at a fixed angle of 165° and at 25 °C.

4. Determination of encapsulation efficiency (EE) and drug loading (DL)

BJO is water insoluble material detectable at an absorption wavelength of 270

nm in ethanol-containing phosphate buffer solution without added sodium alginate. Spongosome nanoparticles were separated from the supernatant using the ultrafiltration centrifugal method. The dispersions were centrifuged for 15 min at 9500 rpm using centrifugal filter tubes (MWCO = 30 kDa; Millipore, USA). It was assumed that the free drug, nonencapsulated in the entrapped nanocarriers, should remain dispersed in the supernatant. The UV-Vis spectrophotometer (UV-1800, Shimadzu, Japan) was set at a wavelength of 270 nm for detection of BJO by its maximal absorption upon addition of ethanol. All experiments were performed at room temperature (25℃).

The encapsulation efficiency (EE) and drug loading (DL) were determined using Equations (1) and (2) below:

$$EE\% = (1 - C_F/C_T) \times 100\% \quad (1)$$

$$DL\% = (C_T - C_F)/C_L \times 100\% \quad (2)$$

where C_T, C_F, and C_L are the total concentration of BJO present in the dispersion system, the concentration of the non-entrapped BJO free drug, and the total concentration of the lipids, respectively.

5. Small angle X-ray scattering experiments

Small angle X-ray scattering (SAXS) experiments were performed at beamline BL19U2 of the National Center for Protein Science Shanghai (NCPSS) at Shanghai Synchrotron Radiation Facility (SSRF). The wavelength, λ, of X-ray radiation was set as 1.033 Å. Scattered X-ray intensities were measured using a Pilatus 1M detector (DECTRIS Ltd). The sample-to-detector distance was set such that the detecting range of momentum transfer q [q=4π sinθ/λ, where 2θ is the scattering angle] of the SAXS experiments was 0.01-0.5Å^{-1}. A flow cell made of a cylindrical quartz capillary with a diameter of 1.5 mm and a wall of 10 μm was used to diminish the radiation damage. The exposure time was set to 1-2 seconds. The X-ray beam was with a size of 0.40 × 0.15 (H x V) mm^2 and was adjusted to pass through the center of the

capillaries for every measurement. Ten 2D images were recorded for each sample and buffer solution in order to obtain good signal-to-noise ratios. The 2D scattering images were converted into 1D SAXS curves through azimuthally averaging procedure after solid angle correction. The normalization by the intensity of the transmitted X-ray beam was done using the BioXTAS RAW software package. [78]

6. Cryogenic transmission electron microscopy (Cryo-TEM)

For cryo-transmission electron microscopy studies, a sample droplet of 2 μL was placed on a lacey carbon-filmed copper grid (Science Services, Muenchen), which was hydrophilized by air plasma glow discharge (Solarus 950, Gatan, Muenchen, Germany) for 30 s. Subsequently, most of the liquid was removed with blotting paper, leaving a thin film stretched over the lace holes. The specimens were instantly shock-frozen by rapid immersion into liquid ethane, cooled to approximately 90 K by liquid nitrogen in a temperature-controlled freezing unit (Zeiss Cryobox, Carl Zeiss Microscopy GmbH, Jena, Germany). The temperature was monitored and kept constant in the chamber during all sample preparation steps. After freezing the specimens, the remaining ethane was removed using blotting paper. The specimen was inserted into a cryo transfer holder (CT3500, Gatan, Muenchen, Germany) and transferred to a Zeiss/Leo EM922 Omega EFTEM (Zeiss Microscopy GmbH, Jena, Germany). Examinations were carried out at temperatures around 90 K. The TEM was operated at an acceleration voltage of 200 kV. Zero-loss filtered images ($\Delta E = 0$ eV) were taken under reduced dose conditions (100–1000 e nm^{-2}). All images were registered digitally by a bottom-mounted CCD camera system (Ultrascan 1000, Gatan, Muenchen，Germany), combined and processed with a digital imaging processing system (Digital Micrograph GMS 1.9, Gatan, Muenchen, Germany).

7. *In vitro* release of BJO

The *in vitro* release studies were performed using the dialysis method.

BJO-spongosomes solution (3 mL) was placed into a dialysis tube with 14 kDa MW cutoff. The latter was incubated in release medium (PBS, pH 7.4; 150 mL) with 0.5 wt% of P80 to enhance the solubility of the released free BJO at 37 ºC. The water bath was equipped with a rotary shaker. 4 mL dissolution medium was taken out at different time points and replace with the same volume of fresh medium. Subsequently, the amount of released BJO was quantified by means of a UV-Vis spectrophotometer (UV-1800, Shimadzu, Japan) at a wavelength 270 nm.

8. *In vitro* cellular cytotoxicity assays

The A549 human lung carcinoma cell line was obtained the American Type Culture Collection (ATCC). The cells were cultured in PRMI-1640 medium supplemented with 10% fetal bovine serum (Gibco, Grand Island, NY, USA) and 1% penicillin at 37 ºC in a humidified atmosphere with 5% CO_2.

Cell viability was measured by 3-(4,5-dimethylthiazol-2-yl)-2,5-diphenyltetrazolium bromide (MTT) assay. The A549 cells were plated in 96-well plates at a density of 5×10^3 cells per well in 100 μL medium. After 24 hours, the growth medium was removed and the cells were exposed during 72 hours to various concentrations of blank spongosomes, free drug BJO, BJO-2, BJO-5 and BJO-10 carriers dispersed in medium with no fetal bovine serum. Then, the culture media were discarded and replaced with fresh culture medium containing 1mg/ml MTT. The incubation lasted another 4 h at 37 ºC. The resulting formazan crystals were solubilized with 100 μL DMSO. The absorbance was measured using a plate enzyme-linked immunosorbent assay reader at 570 nm, with the absorbance at 630 nm as the background correction. The effect of the nanoparticle formulations on the cell proliferation was expressed as cell viability percentages. Untreated cells were considered as 100% viable. The calculation of the IC_{50} value (50% inhibiting concentration) was done by using the Graph Pad Prism software.

9. Cell apoptosis assay

The A549 cells were seeded in 24-well plates (1×10^4 cells/well). After 24 h, the cells were exposed to blank lipid nanocarriers, BJO-loaded nanoparticles, and a solution of the free drug BJO (20μg/mL of BJO) during 72 h. Subsequently, the medium was removed, the cells were washed with cold PBS buffer and a solution of Hoechst 33342 (5μg/mL) was added to the medium towards incubation for 15 min at room temperature. Cold PBS buffer was used to remove the excess dye. The stained cells were analyzed under a fluorescent microscope (ECLIPSE Ti-S, Nikon, Japan) to examine the degree of cell apoptosis.

Results and Discussion

1. Nanoparticle Preparation and Characterization

Spongosomes were fabricated by hydration of melted lipid mixtures in excess aqueous buffer solutions followed by vigorous physical agitation. This fabrication method produced supramolecular structures comparable to other self-assembled GMO-based nanocarrier systems, which have been prepared by either the lipid thin-film-hydration technique [11,73] or *via* hydration of lipid/P80 mixtures homogenized by a heat-treatment procedure using autoclave [65]. The performed SAXS and Cryo-TEM analyses are presented below (Figs. 1 and 2). The employed sample preparation method appeared to be convenient as it avoids the use of organic solvents. The optimal amount of BJO that may be loaded in stable liquid crystalline lipid carriers was determined after systematic experiments. Three self-assembled nanoparticulate formulations were selected as representative for further *in vitro* investigations based on the data for the nanocarriers stability, nanoparticle hydrodynamic sizes, polydispersity index (PDI), drug loading, and encapsulation efficiencies. The results for different nanocarrier compositions, measured at day 1 and day 30 of sample storage, are summarized in Table 2.

Table 2. Physico-chemical characterization of BJO loaded spongosomes at day 1 and day 30 after preparation of the dispersions. The data are presented as the mean values ± standard deviation (SD) (n = 3)

Sample code[#]	Blank		BJO-2		BJO-5		BJO-10	
	Day 1	Day 30	Day 1	Day 30	Day 1	Day 30	Day 1	Day 30
Mean hydrodynamic diameter (nm)	190±1	197±1	174±1	178±1	170±1	175±1	126±1	131±1
PDI	0.195	0.232	0.187	0.206	0.210	0.231	0.230	0.243
Zeta potential（mV）	-25±1	-21±1	-36±1	-35±1	-36±1	-33±1	-32±1	-32±1
EE（%）	-	-	92±1	88±1	89±2	79±1	82±2	62±2
DL（%）	-	-	16±1	16±1	39±1	35±1	72±1	55±2

[#]The sample codes BJO-2, BJO-5, BJO-10 correspond to total BJO concentrations in the samples of 2 mg/ml, 5 mg/ml, and 10 mg/ml, respectively.

Table 2 indicates that the mean hydrodynamic nanoparticle diameters, PDI and zeta potentials of the studied liquid crystalline samples remained almost unchanged during 30 days. It was found that the mean nanoparticle sizes become smaller with the increase of the BJO content. The nanocarriers hydrodynamic volume tended to adopt a more compact configuration with the increase of the BJO content as suggested by the decreased mean nanoparticle size. The stability of the BJO-loaded formulations was confirmed by the measured zeta-potential values (Table 2). The absolute zeta-potential values were relatively elevated for lipid systems. The negative charge on the nanoassemblies may be explained by the adsorbed polymeric alginate shells that surround the nanoparticle cores in addition to the partial charge of the fatty acids at pH 7.4 (negatively charged carboxylic groups of oleic and linoleic acids may be exposed at the nanoparticles surfaces). The repulsion between the P80 coronas of the nanoparticles provided enhanced steric stability of the prepared formulations.

Table 2 also shows that the encapsulation efficiency (EE) of freshly prepared BJO-spongosomes reaches values of 79–92%. The obtained EE results revealed the affinity of the studied lipid matrix for the guest lipophilic BJO ingredient. For BJO-2 samples, no significant changes in the drug loading and encapsulation efficiencies

were observed after 30 days of BJO-2 nanocarriers storage. At variance, the EE values of BJO-5 and BJO-10 samples were less steady with time, which may be due to the saturation of the aqueous lipid dispersion by BJO and phase separation of the oil component on prolonged storage. Data for blank spongosomes confirm the results of previous studies [14,33,66,73]. The latter have indicated that the dispersion of GMO lipid assemblies by amphiphilic polymers results in coexistence of vesicles and larger liquid crystalline nanoparticles with inner nonlamellar organization. Figure 2 below shows that a smaller fraction of vesicles is detected and the population of vesicles is on the decrease upon progressive loading of the oil-type lipophilic drug BJO.

2. Structural analyses of soft nanocarriers loaded with BJO

The effect of BJO loading on the inner organizations of the sponge-type nanocarriers was investigated by SAXS. Representative SAXS patterns at different BJO contents are shown in Fig. 1. The obtained patterns demonstrated that the internal structure of the P80-stabilized nanoparticles does not involve long-range inner crystalline order. Bragg peaks are absent in the SAXS curves, which adopted shapes typical for sponge-type lipid membrane assemblies or precursors of cubosomes [34,65,73]. The blank lipid carrier (lacking BJO) showed a maximum in the large q (0.16 ± 0.01 Å^{-1}) interval (Fig. 1A), which points to the presence of correlated lipid bilayers in the inner organization of the nanoparticles [11]. The defined distance between the lipid membranes (38.41 Å) is linked with the mean aqueous channels thickness in the sponge assemblies [34]. Depending on the molar fraction of P80 and aqueous buffer composition, the first reflection for a GMO bicontinuous cubic phase has been observed in the lower q region (*e.g.* first Bragg peak centred at q = 0.048 – 0.058 Å^{-1} [65,73]), which differs from the features of our obtained SAXS patterns.

The addition of the BJO leads to disappearance of this maximum, *i.e.* there is no more a defined position of the peak of the interacting lipid membranes due to the BJO incorporation in the nanoparticles. The inner water-filled nanochannel structure gets modified and partly disrupted by the uploaded BJO. The SAXS patterns (Fig. 1B-D)

evidence strong intercalation of BJO in the host membrane assemblies. Thus, the BJO appears to be incorporated and well solubilized in the hydrophobic domains of the lipid nanocarriers.

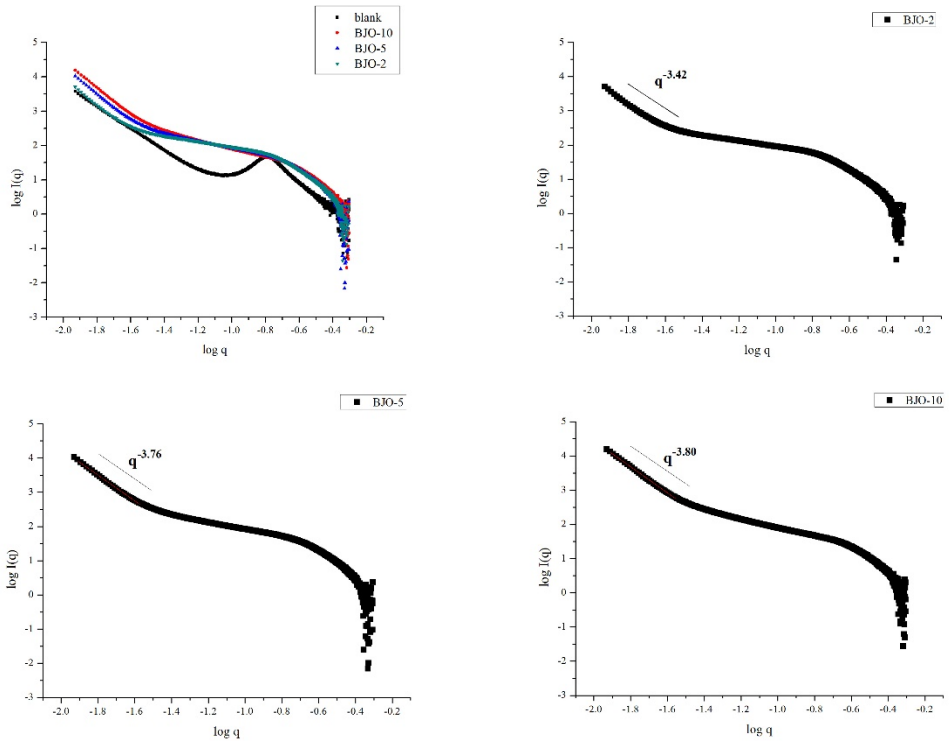

Fig. 1 SAXS patterns of self-assembled blank and BJO loaded lipid nanocarriers at 25 ^{o}C.

To further characterize the inner structure of the BJO loaded nanocarriers, the low-*q* part of the SAXS curves (Fig. 1) was investigated in more detail. The obtained slopes for the BJO-2, BJO-5, and BJO-10 plots were -2.42 (Fig. 1B), -2.76 (Fig. 1C), and -2.80 (Fig. 1D), respectively. These values, between -2 and -3, indicated the formation of dense nanoparticle cores and rough interfaces between the particles and the solvent [79,80]. This result confirmed that BJO loading in the nanocarriers exerts a pronounced influence on the scattering curves. Moreover, the increase in the BJO upload (from Fig. 1B to Fig. 1D) was associated with an increased absolute value of

the slope. This suggests that the BJO-2 carrier has the roughest surface as compared to the BJO-5 and BJO-10 ones.

High resolution Cryo-TEM revealed the morphology of the BJO-loaded spongosomes (Fig. 2). The obtained Cryo-TEM micrographs demonstrated the complex topologies of the drug-loaded liquid crystalline nanoparticles. The nanocarriers were characterized by core–shell structures (Fig. 2, right column). The images confirmed the sponge-type inner organization of the nanoparticles. The nanoparticle core involves a sponge membrane assembly encapsulating BJO, whereas the corona comprises a shell of stabilizing alginate chains. The topology of the surface phase covering the liquid crystalline nanoparticles has been recently discussed in these literatures [33,39,42,65,66,73]. It has been emphasized that the nonlamellar nanoparticles are surrounded by lamellar surface layers upon steric stabilization by amphiphilic stabilizers. The cryo-TEM images revealed that the average size of the studied nanocarriers decreased with the increase of the BJO amount encapsulated in the nanoparticles (Fig. 2, left column). This result is consistent with the DLS data shown in Table 2. Moreover, the density of the core part increased upon encapsulation of BJO. The resulting increased electron density was evidenced by the SAXS data as well (Fig. 1). The established overall morphology of the lipid dispersions reflected the stabilization of the nanocarriers by the P80 corona and by the alginate polyelectrolyte chains.

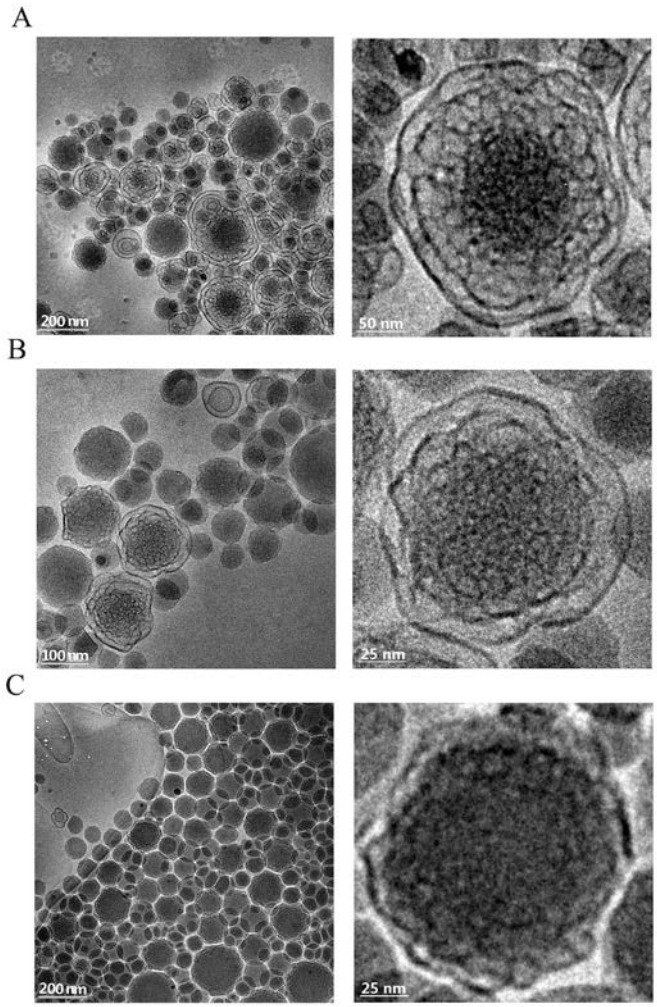

Fig. 2 Cryo-TEM images of BJO-2 (A), BJO-5 (B), and BJO-10 (C) nanocarriers displaying typical sponge-type inner nanoorganization. Left column: the scale bar is 100 nm (A-C). Right column: zoom of up to 6× was performed to visualize the single nanoparticle topologies as a function of the increasing BJO content (A-C).

Recent studies of cellular interaction and toxicity of different types of liquid crystalline nanoparticulate formulations (sponge phase nanoparticles, hexagonal phase nanoparticles, and cubic phase nanoparticles) have demonstrated that the topology plays a role in the efficiency of nanoparticles fusion with membranes and cell membrane destabilization [81,82]. Therefore, it may be expected that the observed nanochannel-type membrane topology of the BJO-2 nanocarriers may affect the interaction of these nanoparticles with cancer cell membranes. The results on apoptotic behaviour of A549 cancer cells are presented below.

3. Drug release and biological evaluations of the nanocarriers at the cellular level

It was expected that the small sizes of the studied drug delivery nanocarriers, established by DLS, will be beneficial for their uptake by tumor cells. The cellular cytotoxicity of BJO-loaded spongosomes was evaluated in human lung carcinoma cell line A549 using an MTT assay. Figure 3 shows that the viability of the A549 cells decreases with the increase in the administered dose of BJO-loaded spongosomes. The viability of A549 cells treated with 12.5 μg/mL and 100 μg/mL pure BJO for 72 h was about 86% and 35%, respectively. The cytotoxicity of BJO-spongosomes against A549 cells was significantly higher than the free BJO in the concentration range from 12.5 to 100 μg/mL. This evidenced the sustained release characteristics of the prepared BJO-spongosomes. Figure 3 revealed that the BJO-2 nanosystem possesses the highest inhibition potential among the studied formulations in terms of anti-cancer apoptotic effect in the indicated concentration range. It may be attributed to the highest encapsulation efficiency of the BJO-2 formulation. Moreover, the specific surface area [79] of the BJO-2 nanoparticles, which is exposed for interaction with the cells, is highest as indicated by the SAXS plots (Fig. 1) and the cryo-TEM investigation of their morphology (Fig. 2).

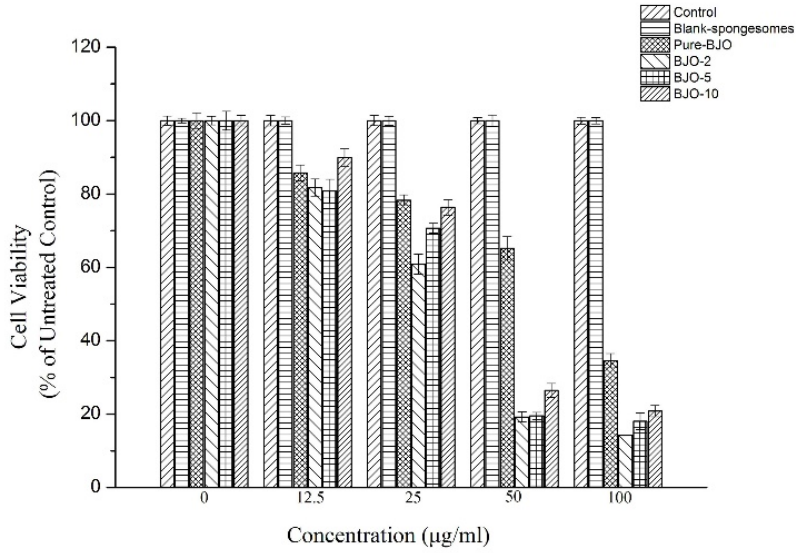

Fig. 3 *In vitro* cytotoxicity of spongosome nanocarriers system against A549 cancer cells determined after 72 h incubation. Cell viability is expressed as the percentage of untreated controls. Data are given as mean ± SD (n = 6).

The determined IC_{50} values of every experimental group are summarized in Table 3. Spongosomes with encapsulated BJO displayed approximately 1.8-2.4 times lower IC_{50} value than that of pure BJO. This result confirms that the BJO-spongosomes may essentially improve the bioavailability of BJO through sustained release. Whereas the blank spongosomes did not show detectable cytotoxicity to the A549 cells at concentrations up to 4 mg/ml after 72 h exposure, the cytotoxicity effect of BJO-2 carriers was particularly evident.

Table 3. IC_{50} values determined upon treatment of A549 cells by spongosome nanocarriers in MTT assays

Treatment group	IC_{50} (μg/mL) (n=3)
Free BJO	68.5±3.1
BJO-2	28.1±3.3
BJO-5	33.3±1.3
BJO-10	37.7±2.7
Blank spongosomes	＞5000

Apoptotic study was performed to estimate the initial cell death [83] occurring with A549 cancer cells exposed to BJO-2 carriers (Fig. 4). Human cancer cells were stained without fixation after incubation with the spongosomes by a DNA-specific fluorescent dye Hoechst 33342, which is appropriate for analysis of living cells undergoing early apoptosis. After Hoechst coloration, nuclei of apoptotic cells appeared bright blue in the fluorescent images (due to chromatin condensation), whereas dark colour may be observed with the nuclei of normal cells. Additional characteristics of cellular apoptosis are the cytoplasm vacuolization, mitochondrial degradation, and DNA fragmentation accompanied by the morphological changes (cell shrinkage) and cellular breakdown into apoptotic bodies [84].

Our results indicated that the A549 cancer cells are intact in the control sample (Fig. 4A). Cells incubated with blank spongosomes showed the same morphology as the control group, which evidenced that the blank spongosomes did not cause cell apoptosis. At variance, the BJO-2 drug-treated A549 cancer cells displayed irregular apoptotic bodies and bright staining (Fig. 4C), which is characteristic of chromatin condensation associated with the apoptosis. Compared with the pure BJO-treated cells (Fig. 4D), the bigger number of brightly blue stained cells observed in Fig. 4C suggested that the degree of DNA condensation and the number of apoptotic bodies in the group treated by BJO-2 carriers had significantly increased.

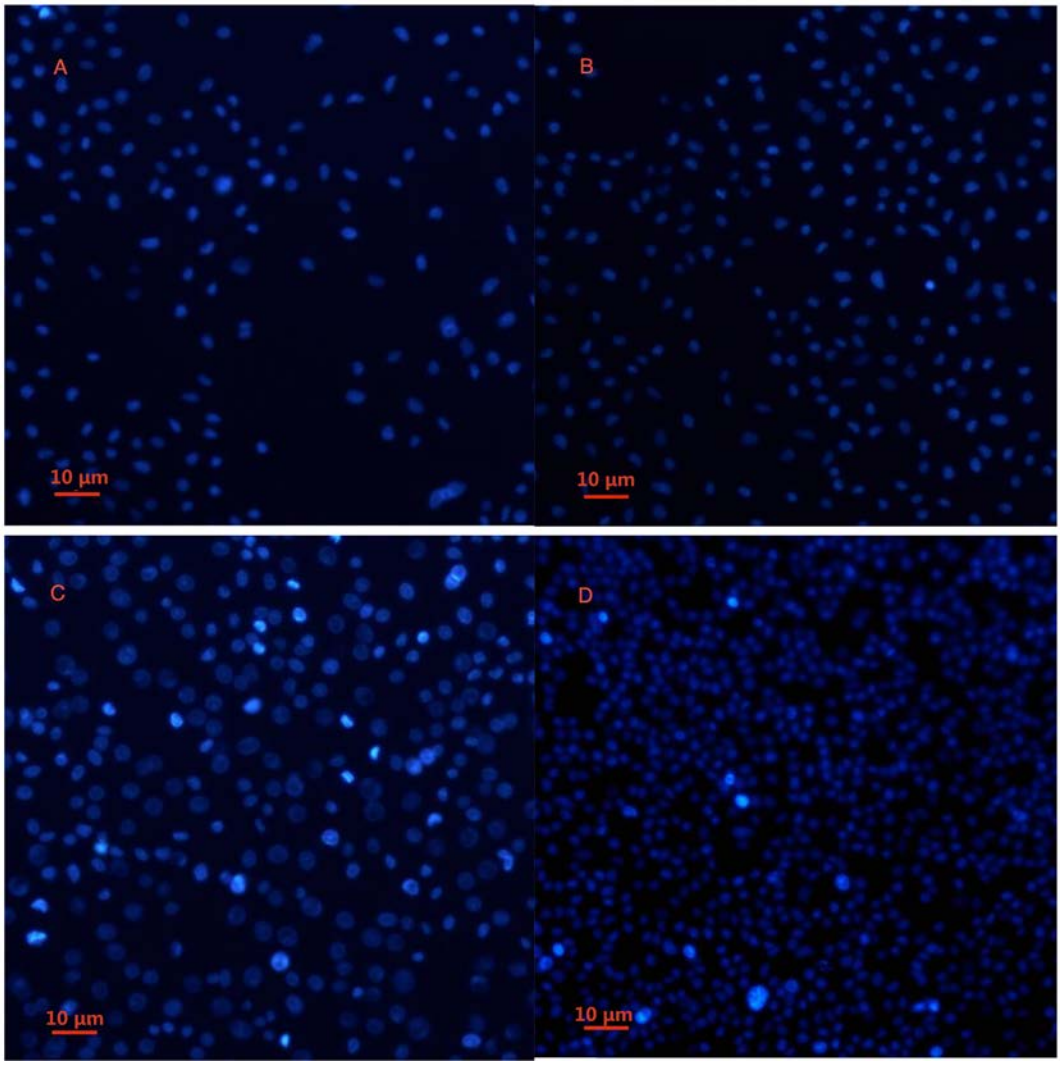

Fig. 4 Effect of four different treatments on the apoptotic behavious of A549 cells. A: Control cells (no treatment); B: Treatment by blank spongosomes; C: BJO-2 nanocarriers; D: Free drug BJO solution. BJO concentration is 20 µg/mL.

The release profiles of BJO from BJO-2 spongosomes were studied *in vitro* using the dialysis method (Fig. 5) in PBS medium (pH=7.4) at 37 ºC. Free drug suspension was investigated as a control. Figure 5 shows that 80% of BJO was released from the free BJO suspension within 10 h, and the accumulative release reached a value of 100% in the following hours. BJO-2 carriers showed a smooth release curve. Notably, no burst release of drug was observed from the BJO-2 nanocarriers. The cumulative release of drug from BJO-2 carriers was 47±2% after 86 hours. This implies that BJO was encapsulated in the spongosome nanocarriers, which ensured the sustained drug

release over time. The observed sustained release may explain the high cytotoxicity of BJO-2 loaded spongosome nanoformulation in the MTT experiments.

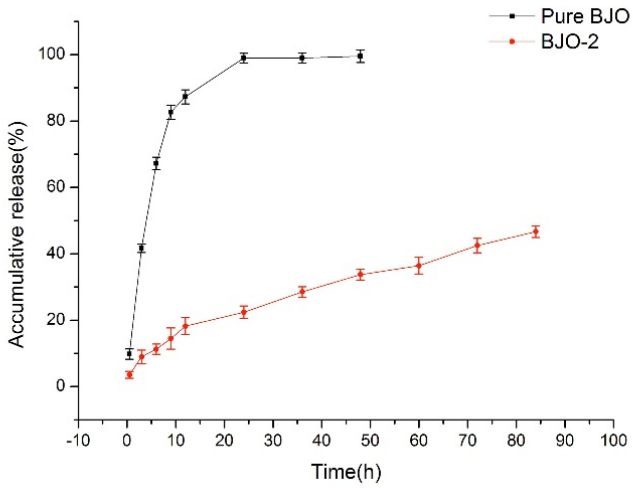

Fig. 5 Comparison of cumulative *in vitro* release of BJO in release medium of PBS (pH=7.4) at 37ºC for BJO-loaded nanocarriers *versus* BJO control. The values are expressed as a mean ± SD (n=3).

The obtained results are in agreement with previous works [15,36,37,72], which have suggested that the internal structure of the nanocarriers is crucial for the drug distribution within the matrix assembly and therefore for the drug release profiles. For instance, single bilayer vesicles may provide significant initial burst release upon lipid bilayer rupture [85,86]. The inner organization of the spongosomes is built-up by randomly ordered bicontinuous lipid membranes. When BJO was incorporated into spongosome nanocarriers, such unique structure can effectively avoid the burst release of BJO and showed a more smooth and sustained release for BJO. Although the system may have some small fraction of vesicles, the behavior is mainly determined by the features of the sponge-type nanocarriers. The sponge-type bicontinuous lipid bilayers within the 3D inner organization of the studied nanocarriers evidently contribute to the sustained release profile of BJO. The internal structure of the

nanocarriers results from intermolecular interactions and packing constrains. In this context, the investigated BJO appeared to be lipophilic and showed high affinity for partitioning in the lipid bilayer membranes building-up the nanocarriers. The created large specific surface area of the lipid/water interfaces inside the spongosome nanoparticles may be suggested to be determinant for the observed sustained drug release.

Conclusion

Spongosomes loaded with anticancer BJO were successfully formulated using self-assembled mixtures of the amphiphilic lipid glycerol monooleate (GMO) and the amphiphile polysorbate 80 (P80) in the presence of alginate polymer (0.5 wt% alginic acid sodium salt) dissolved in the aqueous phase. Optimal drug formulation in nanocarriers was achieved for the BJO-2 system, *i.e.* 2 mg/ml BJO solubilized in the lipid dispersion. The latter was characterized by high encapsulation efficiency and drug loading, long-term stability, and sustained release properties. The obtained IC_{50} values revealed enhancement of the cytotoxicity of BJO encapsulated in spongosomes, *i.e.* IC_{50} for BJO-2 was about 2.4 times higher in comparison to that of the free drug. In addition, BJO-spongosomes considerably increased the number of apoptotic cancer cells, which might result from the improved bioavailability of the drug encapsulated in spongosomes as compared to the BJO alone. The proposed nanotechnology demonstrates considerable potential for translation in Chinese medicine. Therefore, *in vivo* evaluations of the BJO-spongosomes would be the rational perspective of this work.

Acknowledgement：

We gratefully acknowledge the support of this work by Shanghai Natural Science Foundation (Grant No. 15ZR1409900), the National Natural Science Foundation of China (Grant No. 21573070), Fundamental Research Funds for the Central

Universities, National Natural Science Foundation of China (Grant No. 31200617) and Knowledge Innovation Program of CAS (Grant No. 2013KIP103). We thank the staff of the BL19U2 beamline at the National Cencer for Protein Science Shanghai and Shanghai Synchrotron Radiation Facility (Shanghai, People's Republic of China) for assistance during data collection. B.A. was supported by the project ELI - Extreme Light Infrastructure – phase 2 (CZ.02.1.01/0.0/0.0/15_008/0000162) from European Regional Development Fund.

References

[1] Ajazuddin, S. Saraf, Applications of novel drug delivery system for herbal formulations, Fitoterapia 81 (2010) 680–689.

[2] M. Chen, R. Chen, S. Wang, W. Tan, Y. Hu, X. Peng, Y. Wang, Chemical components, pharmacological properties, and nanoparticulate delivery systems of Brucea javanica, Int. J. Nanomed. 8 (2013) 85–92.

[3] S. Ma, F. Chen, X. Ye, Y. Dong, Y. Xue, H. Xu, W. Zhang, S. Song, L. Ai, N. Zhang, W. Pan, Intravenous microemulsion of docetaxel containing an anti-tumor synergistic ingredient (Brucea javanica oil): formulation and pharmacokinetics, Int. J. Nanomed. 8 (2013) 4045–4052.

[4] X.W. Li, H. Wang, W.J. Qin, X. Li, T. Liu, C.M. Fan, Necrosis and apoptosis induced by Brucea Javanica oil emulsion in bladder cancer cell, Chinese Journal of Rehabilitation Theory and Practice 10 (2004) 163–165.

[5] H. Zhang，J.Y. Yang，F. Zhou，L.H. Wang，W. Zhang, Seed Oil of Brucea javanica Induces Apoptotic Death of Acute Myeloid Leukemia Cells via Both the Death Receptors and The Mitochondrial-Related Pathways, Evid-Based Compl. Alt. 5 (2011) 965016.

[6] X. Jiang, Y.Y. Zeng, J.F. Di, X.H. He, Z. Feng, S. Zeng, W.X. Chen, Preliminary studies on the effects of Brucea Javanica emulsion on HPV positive tumor cells form laryngeal papilloma in child, Journal of Jinan University (Medicine Edition) 25 (2004) 408–412.

[7] X.J. Yin, H.Z. Luan, C.L. An, X.L. Wang, Y.Y. Bing, X.N. Wang, Inhibitory effect of Brucea javanica oil emulsion against cervical cancer cell line Hela and its mechanism, Chinese Journal of Cancer Biotherapy 15 (2008) 393–395.

[8] S.Y. Su, Treatment of lung cancer with brain metastasis using an intravenous drip of a 10% emulsion of Brucea javanica seminal oil, Chin. J. Integr. Med. 5 (1985) 86–88.

[9] L. Ma, Y.N. Zhang, Effects of seminal oil emulsion of Brucea javanica on apoptosis and apoptosis-related genes in human hepatocellular carcinoma cells, World

Chinese Journal of Digestology 12 (2004) 559–562.

[10] D.L. He, X.Y. Nan, W.S. Liu, The antitumor effect of 10% Brucea Javanica oil emulsion on prostate cancer cells, Journal of Clinical Urology 9 (1994) 60–62.

[11] Y.Y. Chen, A. Angelova, B. Angelov, M. Drechsler, V.M. Garamus, R. Willumeit-Römer, A.H. Zou, Sterically stabilized spongosomes for multidrug delivery of anticancer nanomedicines, J. Mater. Chem. B 3 (2015) 7734-7744.

[12] Y. Cui, Z. Wu, X. Liu, R. Ni, X. Zhu, L. Ma, J. Liu, Preparation, Safety, Pharmacokinetics, and Pharmacodynamics of Liposomes Containing Brucea javanica Oil, Aaps Pharm. 11 (2010) 878–884.

[13] W. Lv, S. Zhao, H. Yu, N. Li, V.M. Garamus, Y. Chen, P. Yin, R. Zhang, Y. Gong, A. Zou, Brucea javanica oil-loaded nanostructure lipid carriers (BJO NLCs): Preparation, characterization and in vitro, evaluation, Colloids Surf. A 504 (2016) 312-319.

[14] M. Wadsater, J. Barauskas, T. Nylander, F. Tiberg, Formation of Highly Structured Cubic Micellar Lipid Nanoparticles of Soy Phosphatidylcholine and Glycerol Dioleate and Their Degradation by Triacylglycerol Lipase, ACS Appl. Mater. Inter. 6 (2014) 7063–7069.

[15] A. Yaghmur, O. Glatter, Characterization and potential applications of nanostructured aqueous dispersions, Adv. Colloid Interface Sci. 147-148 (2009) 333-342.

[16] E. Esposito, R. Cortesi, M. Drechsler, L. Paccamiccio, P. Mariani, C. Contado, E. Stellin, E. Menegatti, F. Bonina, C. Puglia, Cubosome dispersions as delivery systems for percutaneous administration of indomethacin, Pharm. Res. 22 (2005) 2163-2173.

[17] M. Cohen-Avrahami, A.I. Shames, M.F. Ottaviani, A. Aserin, N. Garti. On the correlation between the structure of lyotropic carriers and the delivery profiles of two common NSAIDs, Colloids Surf. B 122 (2014) 231-240.

[18] A. Yaghmur, B. Sartori, M. Rappolt, The role of calcium in membrane condensation and spontaneous curvature variations in model lipidic systems, Phys. Chem. Chem. Phys. 13 (2011) 3115-3125.

[19] A. Angelova, B. Angelov, R. Mutafchieva, S. Lesieur, Biocompatible

mesoporous and soft nanoarchitectures, J. Inorg. Organomet. Polym. 25 (2015) 214–232.

[20] A. Angelova, M. Ollivon, A. Campitelli, C. Bourgaux, Lipid cubic phases as stable nanochannel network structures for protein biochip development: X-ray diffraction study, Langmuir 19 (2003) 6928–6935.

[21] M. Wadsäter, J. Barauskas, S. Rogers, M.W. Skoda, R.K. Thomas, F. Tiberg, T. Nylander, Structural effects of the dispersing agent polysorbate 80 on liquid crystalline nanoparticles of soy phosphatidylcholine and glycerol dioleate, Soft Matter 11 (2015) 1140-1150.

[22] B. Angelov, A. Angelova, B. Papahadjopoulos-Sternberg, S. Lesieur, J.F. Sadoc, M. Ollivon, P. Couvreur, Detailed structure of diamond-type lipid cubic nanoparticles, J. Am. Chem. Soc. 128 (2006) 5813–5817.

[23] P.T. Spicer. Curr. Opin. Progress in liquid crystalline dispersions: Cubosomes, Curr. Opin. Colloid Interface Sci. 10 (2005) 274-279.

[24] B. Angelov, A. Angelova, V.M. Garamus, M. Drechsler, R. Willumeit, R. Mutafchieva, P. Štěpánek, S. Lesieur, Earliest stage of the tetrahedral nanochannel formation in cubosome particles from unilamellar nanovesicles, Langmuir 28 (2012) 16647–16655.

[25] W.T. Góźdź, Cubosome Topologies at Various Particle Sizes and Crystallographic Symmetries, Langmuir 31 (2015) 13321-13326.

[26] C.E. Conn, C.J. Drummond, Nanostructured bicontinuous cubic lipid self-assembly materials as matrices for protein encapsulation, Soft Matter 9 (2013) 3449-3464.

[27] A. Misiunas, G. Niaura, J. Barauskas, R. Meskys, R. Rutkiene, V. Razumas, T. Nylander, Horse heart cytochrome c entrapped into the hydrated liquid-crystalline phases of phytantriol: X-ray diffraction and Raman spectroscopic characterization, J. Colloid Interface Sci. 378 (2012) 232–240.

[28] C.V. Kulkarni, T.Y. Tang, A.M. Seddon, J.M. Seddon, O. Ces, R.H. Templer, Engineering bicontinuous cubic structures at the nanoscale-the role of chain splay,Soft Matter 6 (2010) 3191-3194.

[29] A. Angelova, B. Angelov, B. Papahadjopoulos-Sternberg, C. Bourgaux, P. Couvreur, Protein driven patterning of self-assembled cubosomic nanostructures: Long oriented nanoridges, J. Phys. Chem. B 109 (2005) 3089-3093.

[30] N. Tran, X. Mulet, A.M. Hawley, C.E. Conn, J.L. Zhai, L.J. Waddington, C.J. First Direct Observation of Stable Internally Ordered Janus Nanoparticles Created by Lipid Self-Assembly, Nano Lett. 15 (2015) 4229-4233.

[31] A. Angelova, B. Angelov, M. Drechsler, V.M. Garamus, S. Lesieur, Protein entrapment in PEGylated lipid nanoparticles, Int. J. Pharm. 454 (2013) 625–632.

[32] Y.D. Dong, A.J. Tilley, I. Larson, M.J. Lawrence, H. Amenitsch, M. Rappolt, T. Hanley, B.J. Boyd, Nonequilibrium Effects in Self-Assembled Mesophase Materials: Unexpected Supercooling Effects for Cubosomes and Hexosomes, Langmuir 26 (2010) 9000–9010.

[33] C. Nilsson, J. Østergaard, S.W. Larsen, C. Larsen, A. Urtti, A. Yaghmur, PEGylation of phytantriol-based lyotropic liquid crystalline particles--the effect of lipid composition, PEG chain length, and temperature on the internal nanostructure, Langmuir 30 (2014) 6398-6407.

[34] B. Angelov, A. Angelova, R. Mutafchieva, S. Lesieur, U. Vainio, V.M. Garamus, G. Jensen, J.S. Pedersen, SAXS investigation of a cubic to a sponge (L_3) phase transition in self-assembled lipid nanocarriers, Phys. Chem. Chem. Phys., 13 (2011) 3073-3081.

[35] B. Angelov, A. Angelova, U. Vainio, V.M. Garamus, S. Lesieur, R. Willumeit, P. Couvreur, Long living intermediates during a lamellar to a diamond-cubic lipid phase transition: A small-angle X-ray scattering investigation, Langmuir 25 (2009) 3734-3742.

[36] X. Mulet, B.J. Boyd, C.J. Drummond, Advances in drug delivery and medical imaging using colloidal lyotropic liquid crystalline dispersions, J. Colloid Interface Sci. 393 (2013) 1−20.

[37] A. Zabara, R. Mezzenga, Controlling molecular transport and sustained drug release in lipid-based liquid crystalline mesophases, J. Control. Release 188 (2014) 31-43.

[38] B. Angelov, A. Angelova, B. Papahadjopoulos-Sternberg, S.V. Hoffmann, V. Nicolas, S. Lesieur, Protein-containing PEGylated cubosomic particles: Freeze-fracture electron microscopy and synchrotron radiation circular dichroism study, J. Phys. Chem. B, 116 (2012) 7676−7686.

[39] B. Angelov, A. Angelova, S.K. Filippov, M. Drechsler, P. Štěpánek, S. Lesieur, Multicompartment lipid cubic nanoparticles with high protein upload: millisecond dynamics of formation, ACS Nano 8 (2014) 5216–5226.

[40] N. Garti, G. Hoshen, A. Aserin, Lipolysis and structure controlled drug release from reversed hexagonal mesophase, Colloids Surf. B 94 (2012) 36-43.

[41] E. Esposito, L. Ravani, P. Mariani, C. Contado, M. Drechsler, C. Puglia, R. Cortesi, Curcumin containing monoolein aqueous dispersions: a preformulative study, Mat. Sci. Eng. C Mater. 33 (2013) 4923-4934.

[42] B. Angelov, A. Angelova, M. Drechsler, V. M. Garamus, R. Mutafchieva, S. Lesieur, Identification of large channels in cationic PEGylated cubosome nanoparticles by synchrotron radiation SAXS and Cryo-TEM imaging, Soft Matter 11 (2015) 3686-3692.

[43] Z. Almsherqi, S. Hyde, M. Ramachandran, Y. Deng, Cubic membranes: a structure-based design for DNA uptake, J. R. Soc. Interface 5 (2008) 1023–1029.

[44] G. Zhen, T.M. Hinton, B.W. Muir, S. Shi, M. Tizard, K.M. McLean, P.G. Hartley, Glycerol Monooleate-Based Nanocarriers for siRNA Delivery in Vitro, P. Gunatillake, 9 (2012) 2450–2457.

[45] E. Nazaruk, P. Miszta, S. Filipek, E. Gorecka, E.M. Landau, R. Bilewicz, Lyotropic Cubic Phases for Drug Delivery: Diffusion and Sustained Release from the Mesophase Evaluated by Electrochemical Methods, Langmuir 31 (2015) 12753-12761.

[46] M. Cano−Sarabia, A. Angelova, N. Ventosa, S. Lesieur, Cholesterol induced CTAB micelle-to-vesicle phase transitions, J. Colloid Interf. Sci. 350 (2010) 10−15.

[47] S. Jain, N. Bhankur, N.K. Swarnakar, K. Thanki, Phytantriol Based “Stealth” Lyotropic Liquid Crystalline Nanoparticles for Improved Antitumor Efficacy and Reduced Toxicity of Docetaxel, Pharm. Res. 32 (2015) 3282-3292.

[48] A. Angelova, B. Angelov, M. Drechsler, S. Lesieur, Neurotrophin delivery using nanotechnology, Drug Discovery Today, 18 (2013) 1263–1271.

[49] A. Yaghmur, M. Rappolt, S.W. Larsen, In situ, forming drug delivery systems based on lyotropic liquid crystalline phases: structural characterization and release properties, J. Drug Deliv. Sci. Tec. 23 (2013) 325-332.

[50] A. Angelova, B. Angelov, B. Papahadjopoulos-Sternberg, M. Ollivon, C. Bourgaux, Structural organization of proteocubosome carriers involving medium- and large-size proteins, J. Drug Deliv. Sci. Tec. 15 (2005) 108–112.

[51] S. Phan, W.K. Fong, N. Kirby, T. Hanley, B.J. Boyd, Evaluating the link between self-assembled mesophase structure and drug release, Int. J. Pharm. 421 (2011) 176-182.

[52] A. Angelova, B. Angelov, S. Lesieur, R. Mutafchieva, M. Ollivon, C. Bourgaux, R. Willumeit, P. Couvreur, Dynamic control of nanofluidic channels in protein drug delivery vehicles, J. Drug Deliv. Sci. Tec. 18 (2008) 41-45.

[53] Z. Yang, Y. Tan, M. Chen, L. Dian, Z. Shan, X. Peng, C. Wu, Development of Amphotericin B-Loaded Cubosomes Through the SolEmuls Technology for Enhancing the Oral Bioavailability, Aaps Pharm. 13 (2012) 1483-1491.

[54] H.H. Shen, V. Lake, A.P.L. Brun, M. James, A.P. Duff, Y. Peng, K.M. McLean, P.G. Hartley, Targeted detection of phosphatidylserine in biomimetic membranes and invitro cell systems using annexin V-containing cubosomes, Biomaterials 34 (2013) 8361-8369.

[55] A. Tan, S. Simovic, A.K. Davey, T. Rades, B.J. Boyd, C.A. Prestidge, Silica nanoparticles to control the lipase-mediated digestion of lipid-based oral delivery systems, Mol. Pharmaceutics 7 (2010) 522-532.

[56] A. Chemelli, B. Conde-Valentin, F. Uhlig, O. Glatter, Amino Acid Induced Modification of Self-Assembled Monoglyceride-Based Nanostructures, Langmuir 31 (2015) 10377-10381.

[57] J. Zhai, L. Waddington, T.J. Wooster, M.I. Aguilar, B.J. Boyd, Revisiting β-casein as a stabilizer for lipid liquid crystalline nanostructured particles, Langmuir 27 (2011) 14757-14766.

[58] S. Peng, P.G. Hartley, T.C. Hughes, Q. Guo, Enhancing thermal stability and mechanical properties of lyotropic liquid crystals through incorporation of a polymerizable surfactant, Soft Matter 11 (2015) 6318-6326.

[59] C.G. Park, Y.K. Kim, Y.B. Choy, Mucoadhesive microparticles with a nanostructured surface for enhanced bioavailability of glaucoma drug, J. Control. Release 220 (2015) 180-188.

[60] K. Liu, R. Xing, Q. Zou, G. Ma, H. Möhwald, X. Yan, Simple peptide-tuned self-assembly of photosensitizers towards anticancer photodynamic therapy, Angew. Chem. Int. Ed. 55 (2016) 3036-3039.

[61] H. Zhang, J. Fei, X. Yan, A. Wang, J. Li, Enzyme-responsive release of doxorubicin from monodisperse dipeptide-based nanocarriers for highly efficient cancer treatment in vitro, Adv. Func. Mater. 25 (2015) 1193-1204.

[62] F. Zhao, G. Shen, C. Chen, R. Xing, Q. Zou, G. Ma, X. Yan, Nanoengineering of stimuli-responsive protein-based biomimetic protocells as versatile drug delivery tools, Chemistry - A European J. 20 (2014) 6880-6887.

[63] C. Chen, S. Li, K. Liu, G. Ma, X. Yan, Co-assembly of heparin and polypeptide hybrid nanoparticles for biomimetic delivery and anti-thrombus therapy. Small 12 (2016) 4719-25.

[64] A.R. Patel, M. Chougule, M. Singh, EphA2 targeting pegylated nanocarrier drug delivery system for treatment of lung cancer, Pharm. Res. 31 (2014) 2796-2809.

[65] M. Valldeperas, M. Wisniewska, M. Ram-On, E. Kesselman, D. Danino, T. Nylander, J. Barauskas, Sponge phases and nanoparticle dispersions in aqueous mixtures of mono- and diglycerides, Langmuir 32 (2016) 8650-8659.

[66] H. Azhari, M. Strauss, S. Hook, B. Boyd, S. B. Rizwan, Stabilising cubosomes with Tween 80 as a step towards targeting lipid nanocarriers to the blood-brain barrier, Eur. J. Pharm. Biopharm., 104 (2016) 148-155.

[67] I. D. M. Azmi, P.P. Wibroe, L. P. Wu, A. I. Kazem, H. Amenitsch, S. M. Moghimi, A. Yaghmur, A structurally diverse library of safe-by-design citrem-phospholipid lamellar and non-lamellar liquid crystalline nano-assemblies, J. Control. Release 239 (2016) 1-9.

[68] M. Younus, R. N. Prentice, A.N. Clarkson, B.J. Boyd, S.B. Rizwan, Incorporation of an endogenous neuromodulatory lipid, oleoylethanolamide, into Cubosomes: Nanostructural characterization, Langmuir 32 (2016) 8942-8950.

[69] M. D. Chatzidaki, K. Papadimitriou, V. Alexandraki, E. Tsirvouli, Z. Chakim, A. Ghazal, K. Mortensen, A. Yaghmur, S. Salentinig, V. Papadimitriou, E. Tsakalidou, A. Xenakis, Microemulsions as potential carriers of nisin: Effect of composition on structure and efficacy, Langmuir 32 (2016) 8988-8998.

[70] N. A. Elgindy, M. M. Mehanna, S. M. Mohyeldin, Self-assembled nano-architecture liquid crystalline particles as a promising carrier for progesterone transdermal delivery, Int. J. Pharm. 501 (2016) 167-179.

[71] S. Saesoo, S. Bunthot, W. Sajomsang, P. Gonil, S. Phunpee, P. Songkhum, K. Laohhasurayotin, T. Wutikhun, T. Yata, U.R. Ruktanonchai, N. Saengkrit, Phospholipid-chitosan hybrid nanoliposomes promoting cell entry for drug delivery against cervical cancer, J. Colloid Interface Sci. 480 (2016) 240-248.

[72] N. B. Bisset, B. J. Boyd, Y.-D. Dong, Tailoring liquid crystalline lipid nanomaterials for controlled release of macromolecules, Int. J. Pharm. 495 (2015) 241-248.

[73] L. Zerkoune, S. Lesieur, J.-L. Putaux, L. Choisnard, A. Gèze,D. Wouessidjewe, B. Angelov, C. Vebert-Nardin, J. Doutch, A. Angelova, Mesoporous self-assembled nanoparticles of biotransesterified cyclodextrins and nonlamellar lipids as carriers of water-insoluble substances, Soft Matter 12 (2016) 7539-7550.

[74] S. P. Akhlaghi, I.R. Ribeiro, B.J. Boyd, W. Loh, Impact of preparation method and variables on the internal structure, morphology, and presence of liposomes in phytantriol-Pluronic® F127 cubosomes, Colloids and Surfaces B: Biointerfaces 145 (2016) 845-853.

[75] A. Linkeviciute, A. Misiunas, E. Naujalis, J. Barauskas, Preparation and characterization of quercetin-loaded lipid liquid crystalline systems, Colloids and Surfaces B: Biointerfaces, 2015 128, 296-303.

[76] V. I. Petrenko, V. L. Aksenov, M. V. Avdeev, L. A. Bulavin, L. Rosta, L. Vekas, V. M. Garamus, R. Willumeit, Analysis of the structure of aqueous ferrofluids by the

small-angle neutron scattering method, Physics of the Solid State, 52 (2010) 974–978.

[77] V.I. Petrenko, M.V. Avdeev, V.M. Garamus, L.A. Bulavin, V.L. Aksenov, L. Rosta, Micelle formation in aqueous solutions of dodecylbenzene sulfonic acid studied by small-angle neutron scattering, Colloids and Surfaces A: Physicochem. Eng. Aspects, 369 (2010) 160–164.

[78] S.S. Nielsen, K.N. Toft, D. Snakenborg, M.G. Jeppesen, J.K. Jacobsen, B. Vestergaard, J.P. Kutter, L. Arleth, BioXTAS RAW , a software program for high-throughput automated small-angle X-ray scattering data reduction and preliminary analysis, J. Appl. Crystallogr. 42 (2009) 959-964.

[79] D. Avnir (Ed.), The Fractal Approach to Heterogeneous Chemistry, Wiley, New York, 1989.

[80] K. Oehlke, V.M. Garamus, A. Heins, H. Stöckman, K. Schwarz, The partitioning of emulsifiers in o/w emulsions: A comparative study of SANS, ultrafiltration and dialysis, J. Colloid Interface Sci. 322 (2008) 294−303.

[81] J. Barauskas, C. Cervin, M. Jankunec, M. Spandyreva, K. Ribokaite, F. Tiberg, M. Johnsson, Interactions of lipid-based liquid crystalline nanoparticles with model and cell membranes. Int. J. Pharm. 391 (2010) 284−291.

[82] T. M. Hinton, F. Grusche, D. Acharya, R. Shukla, V. Bansal, L. J. Waddington, P. Monaghana, B.W. Muir, Bicontinuous cubic phase nanoparticle lipid chemistry affects toxicity in cultured cells, Toxicol. Res. 3 (2014) 11-22.

[83] G. Yang, T. Yang, W. Zhang, M. Lu, X. Ma, G.Y. Xiang, In vitro and in vivo antitumor effects of folate-targeted ursolic acid stealth liposome, J. Agric. Food Chem. 62 (2014) 2207-2215.

[84] S.J. Heo, K.N. Kim, W.J. Yoon, C. Oh, A. Affan, Y.J. Lee, H.S. Lee, D.H. Kang, Chromene induces apoptosis via caspase-3 activation in human leukemia HL-60 cells, Food Chem. Toxicol. 49 (2011) 1998-2004.

[85] O. Allerbo, A. Lundström, K. Dimitrievski, Simulations of lipid vesicle rupture induced by an adjacent supported lipid bilayer patch, Colloids and Surfaces B: Biointerfaces, 82 (2011) 632-636.

[86] P. Prabhakara, T. Zenia, K. Marina, K.P. Shama, S.N. Girish, N.H. Matapady,

Preparation and evaluation of lipid vesicles of camptothecin as targeted drug delivery system, Pak. J. Pharm. Sci. 26 (2013) 779-786.